

Ultrafast switching of hard X-rays

Peter Gaal,^{a*} Daniel Schick,^b Marc Herzog,^b André Bojahr,^b Roman Shayduk,^a Jevgeni Goldshteyn,^b Wolfram Leitenberger,^b Ionela Vrejoiu,^c Dmitry Khakhulin,^d Michael Wulff^d and Matias Bargheer^{a,b}

^aHelmholtz-Zentrum Berlin für Materialien und Energie GmbH, Wilhelm-Conrad-Röntgen Campus, BESSY II, Albert-Einstein-Strasse 15, 12489 Berlin, Germany, ^bInstitut für Physik und Astronomie, Universität Potsdam, Karl-Liebknecht-Strasse 24-25, 14476 Potsdam, Germany, ^cMax-Planck-Institut für Mikrostrukturphysik, Weinberg 2, 06120 Halle, Germany, and ^dEuropean Synchrotron Radiation Facility (ESRF), 6 rue Jules Horowitz, 38000 Grenoble, France.

*E-mail: peter.gaal@helmholtz-berlin.de

A new concept for shortening hard X-ray pulses emitted from a third-generation synchrotron source down to few picoseconds is presented. The device, called the PicoSwitch, exploits the dynamics of coherent acoustic phonons in a photo-excited thin film. A characterization of the structure demonstrates switching times of ≤ 5 ps and a peak reflectivity of $\sim 10^{-3}$. The device is tested in a real synchrotron-based pump–probe experiment and reveals features of coherent phonon propagation in a second thin film sample, thus demonstrating the potential to significantly improve the temporal resolution at existing synchrotron facilities.

Keywords: ultrafast X-ray diffraction; thin film; coherent phonons; X-ray switching; pulse shortening; optical pump X-ray probe; time-resolved.

© 2014 International Union of Crystallography

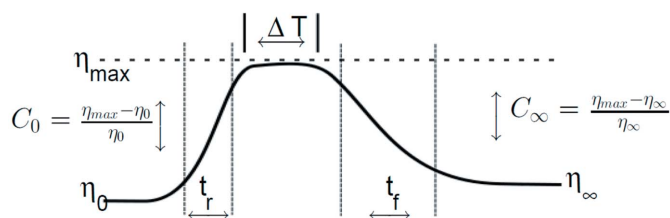
1. Introduction

Ultrafast structural dynamics can be monitored by time-resolved X-ray techniques, provided that the probing X-ray pulse is sufficiently short (Bargheer *et al.*, 2006; Rousse *et al.*, 2001). Unfortunately, large-scale facilities like synchrotrons, which offer the best experimental conditions in terms of stability, tunability and brilliance, typically do not deliver pulses shorter than 100 ps. An exception is the so-called low- α mode (Abo-Bakr *et al.*, 2002), where the synchrotron is able to generate pulses as short as 5 ps. However, the low- α mode is only available for a few weeks per year, since it reduces the X-ray intensity at all beamlines connected to the storage ring. To date, various schemes exist that can manipulate or resolve the time structure of a synchrotron X-ray pulse. All of them are indirect in the sense that they do not act on the X-ray pulse itself. Either the electron bunch in the storage ring is manipulated [*e.g.* femtoslicing (Schoenlein *et al.*, 2000; Beaud *et al.*, 2007) or orbit deflection using RF cavities (Zholents *et al.*, 1999)], or electrons generated in photocathodes are used to spatially map the temporal structure of the synchrotron pulse on a screen (Enquist *et al.*, 2010; Chang *et al.*, 1996). The highest temporal resolution at synchrotron sources is obtained by using electron slicing schemes, which leads to 150 fs pulses (Schoenlein *et al.*, 2000; Beaud *et al.*, 2007). However, these schemes result in a rather low photon flux. Highly improved experimental conditions are found at new facilities like free-electron-laser (FEL) sources (Emma *et al.*, 2010; Pile, 2011;

Geloni *et al.*, 2010). However, the large demand for ultrashort, brilliant and stable X-ray pulses from the ultrafast community is not yet satisfied.

Several early attempts were made to manipulate the time structure of the synchrotron X-ray pulse directly. Early experiments reported switching of hard X-rays resulting in pulses of 100 ps duration and more (Wark *et al.*, 1989; Zolotoyabko & Quintana, 2004; Allam, 1970; Grigoriev *et al.*, 2006; Navirian *et al.*, 2011). A promising concept is based on optical phonons (Bucksbaum & Merlin, 1999); however, this could not yet be realised experimentally (Sheppard *et al.*, 2005). A modified approach exploiting zone-folded acoustic phonons in a superlattice (Herzog *et al.*, 2010) demonstrated a modulation of the switching-contrast ratio of $\Delta R/R = 24.1$ during 1 ps. However, the first modulation maximum is followed by several post-pulses that result from the generation of multiple sound waves at interfaces between the superlattice layers. This leads to a significant protraction of the switching time.

Here we present a new concept that builds on the experience of previous approaches. We excite coherent strain waves in a thin metallic oxide film in order to modify the diffraction efficiency of the structure at a fixed Bragg angle on a picosecond time scale. An exemplary gate is shown in Fig. 1. A good switch provides short rise and fall times t_r and t_f and a short on-time ΔT . Also the diffraction efficiency before (η_0) and after (η_∞) the switching should be low, whereas it should be high in the on-state (η_{\max}). This automatically increases the switching contrast C_0 and C_∞ . The contrast is defined as $C_i =$


Figure 1

Gate parameters defining the performance of an X-ray switch: turn-on time ΔT , rise- and fall-time t_r and t_f , respectively, diffraction efficiency before (η_0), during (η_{\max}) and after (η_∞) switching and contrast before (C_0) and after (C_∞) switching.

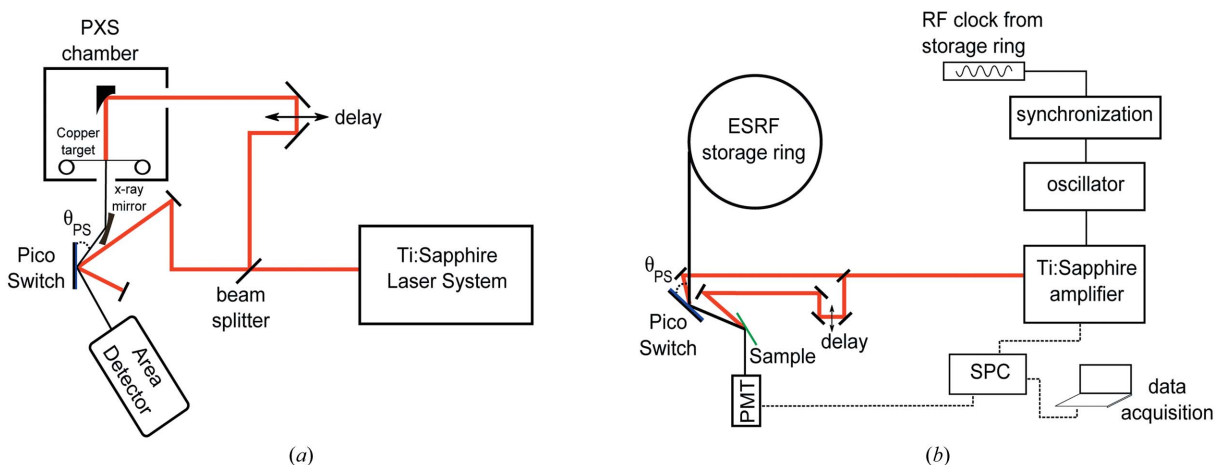
$(\eta_{\max} - \eta_i) / \eta_i$ ($i = 0, \infty$). After introducing the experimental method of ultrafast X-ray diffraction (UXRD) in the next section, we present a full characterization of the PicoSwitch both experimentally and theoretically in §3. In §4 we apply our approach to a real synchrotron-based ultrafast pump–probe experiment. Results of this experiment are discussed in §5.

2. Experimental set-ups

We performed UXRD experiments at the Plasma X-ray Source (PXS) (Schick *et al.*, 2012, 2013) at the University of Potsdam and at the ID09B beamline at the European Synchrotron Radiation Facility (ESRF) in Grenoble, France. Schematics of the set-ups are shown in Figs. 2(a) and 2(b), respectively. A high-power laser yielding ultrashort laser pulses is employed to excite the sample and the PicoSwitch, respectively. At the University of Potsdam we use a commercial Coherent Legend Duo system which provides optical pulses ($\lambda = 800$ nm, pulse energy = 8 mJ) with a duration of 40 fs at a repetition rate of 1 kHz. For X-ray generation, the laser pulses are focused onto a copper target in a vacuum chamber. The target is wrapped on a system of

spools together with debris protection tape. Interaction of the highly intense laser pulses with the copper target leads to the emission of characteristic Cu K_α X-ray ($E = 8.047$ keV) bursts of 150 fs duration (Schick *et al.*, 2012; Zamponi *et al.*, 2009). The temporal delay between optical pump and X-ray probe pulses is realised by a mechanical delay stage. Since the X-ray probe pulse is generated by the same laser as the pump beam, both are perfectly synchronized. X-ray photons, which are emitted in a solid angle of 4π , are collected using a Montel X-ray focusing mirror having an image ratio of 1:7. The mirror is mounted 875 mm from the sample. The 4π emission angle, the energy bandwidth and the focal distance reduce the angular resolution to approximately 0.1° in a diffraction experiment in convergence correction mode (Schick *et al.*, 2013), as indicated by the gray shaded area in Figs. 4(d) and 4(e). Reflected X-ray photons from the sample are detected with a CMOS hybrid-pixel area detector (Dectris Pilatus 100K).

For the experiments at the ID09B beamline at the ESRF the storage ring was running in 16-bunch mode, delivering monochromated X-ray pulses at an energy of 12 keV and a duration of 90–120 ps (Camarata *et al.*, 2009). The beamline is equipped with a commercial laser system (Coherent Legend) which yields 800 nm optical pulses with an energy of 1.5 mJ and a duration of 600 fs at a repetition rate of 1 kHz. The laser oscillator was electronically phase-locked to the synchrotron repetition rate, which allows for timing the delay t between the amplified optical and X-ray pulses with an accuracy of better than 5 ps. This is significantly shorter than the X-ray pulse duration. The gated probe pulse reflected by the PicoSwitch is inherently synchronized to the pump laser after switching. For the second optical path, a mechanical delay stage has been introduced to realise the pump–probe delay τ . X-ray photons have been detected with a plastic scintillator (BC408, Saint-Gobain) attached to a Hamamatsu


Figure 2

(a) Typical UXRD set-up. The PXS at the University of Potsdam delivers 150 fs X-ray pulses at an energy of 8.047 keV. A detailed description of the PXS is given by Schick *et al.* (2012) and Zamponi *et al.* (2009). Laser parameters are: pulse energy 8 mJ, pulse duration 40 fs and repetition rate 1 kHz. The pump fluence was set to 30 mJ cm^{-2} . (b) Synchrotron-based pump–probe experiment. A Ti:sapphire laser system (Coherent Legend) is synchronized to the repetition rate of the ESRF storage ring with an accuracy of ≤ 5 ps between the X-ray and laser pulses. Laser parameters are: pulse energy 1.5 mJ, pulse duration 600 fs and repetition rate 1 kHz. The pump–probe scheme is shown in Fig. 4(a) in detail. X-ray photons diffracted from the sample are captured in a photomultiplier (PMT) and counted in a single-photon-counting (SPC) unit.

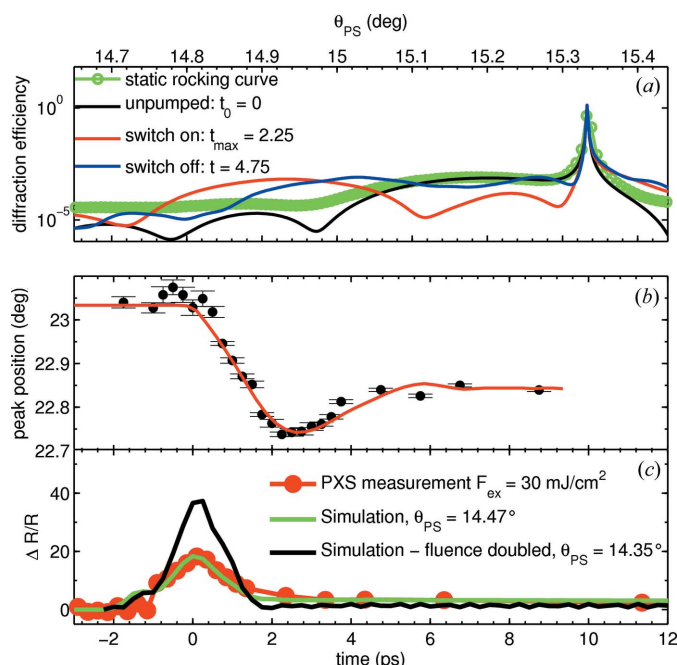


Figure 3 Characterization of the PicoSwitch. (a) Green: measured diffraction curve of the PicoSwitch. The data were recorded at the ID09B beamline at ESRF at an X-ray energy of 12 keV. Black: simulation of the unexcited structure; red: simulation for maximum layer expansion 2.25 ps after optical excitation; blue: simulation at $t = 4.75$ ps after optical excitation. At this delay all coherent sound waves have propagated into the substrate. (b) Ultrafast shift of the layer peak measured at the PXS at the University of Potsdam with an X-ray energy of 8.047 keV. The red curve shows a simulation of the coherent phonon dynamics. (c) Measurement (red bullets) and simulations (green and black solid lines) of the PicoSwitch. The measurement was performed at the Plasma X-ray Source (PXS) at the University of Potsdam. The simulation (green line) shows excellent agreement with the measured data. A larger contrast and switching efficiency is predicted for higher pump fluences (black line). The angle θ_{PS} is the X-ray diffraction angle as defined in Fig. 2(a).

photomultiplier tube (H7422). The detector signal was fed to a single-photon-counting unit controlled by computer.

It is important to note that the different X-ray energies used during the PXS and the ESRF experiments lead to two different angular ranges in the diffraction data presented in this contribution. We preserved the original angular scales to clearly distinguish the different experiments. The X-ray response of the sample is essentially the same for both X-ray energies used in the experiments. All diffraction data shown were recorded on the (002) reflection of SrTiO₃ (STO) (substrate peak) and SrRuO₃ (SRO) (layer peak). At an X-ray energy of 12 keV, the maximum of the (002) reflection of SRO appears at 15.2° (Fig. 3a). These data were recorded at the ESRF. At an X-ray energy of 8.047 keV, the SRO layer peak appears at 23.03° (Fig. 3b). These data were recorded at the PXS at the University of Potsdam.

3. PicoSwitch characterization

The PicoSwitch consists of a thin SRO layer with a thickness of $d_{SRO} = 15.4$ nm which was epitaxially grown on an STO substrate (Vrejoiu *et al.*, 2006). A static $\theta/2\theta$ scan recorded at

the ID09B beamline at the ESRF is shown by the green line in Fig. 3(a). Note in particular that the peak reflectivity of the (002) SRO reflection at X-ray energies from 8 keV to 12 keV is $\sim 10^{-3}$. This corresponds to the highest achievable diffraction efficiency in the on-state, as defined in Fig. 1. The black line is a simulation of the diffraction profile from the structure using dynamic diffraction theory (Als-Nielsen, 2011).

To record the ultrafast response of the PicoSwitch to the optical excitation, we resort to the UXRD set-up at the PXS at the University of Potsdam (Schick *et al.*, 2012). Fig. 3(b) shows the shift of the SRO layer peak as a function of the delay after excitation of the PicoSwitch with an ultrashort 800 nm pump pulse. The interpretation of coherent phonon dynamics of an excited layer is straightforward (Sokolowski-Tinten *et al.*, 2001) and the red solid line shows a simulation using a linear-chain model (Herzog *et al.*, 2012b). Excitation of the PicoSwitch with an ultrashort optical pulse launches coherent expansion waves starting at the air/SRO and SRO/STO interfaces through the SRO layer, shifting the layer Bragg peak to lower angles. The expansion waves propagate at the sound velocity in SRO of $v_{SRO} = 6.3$ nm ps⁻¹ (Herzog *et al.*, 2012a; Schick *et al.*, 2014). Reflection of the strain wave at the surface converts the expansion that was launched at the SRO/STO interface into a compression wave, which propagates back through the layer and into the substrate, thus shifting the Bragg peak back to about two-thirds compared with the maximum expansion. Due to the perfect matching of the acoustic impedances of SRO and STO (Herzog *et al.*, 2012a), there is no reflection at the interface. The coherent dynamics in the SRO film last for $\tau_{switch} = 2d_{SRO}/v_{SRO} \leq 5$ ps, *i.e.* the time it takes for the strain waves to propagate back and forth through the layer. For later times the peak position is given by the remaining heat expansion, and heat conduction cools the layer on a nanosecond timescale (Shayduk *et al.*, 2011). Hence, there is an angular range, which extends from 22.85° to 22.75° in Fig. 3(b), where the ultrafast coherent phonon propagation is responsible for the rise and fall of the diffraction efficiency. This range can be exploited for ultrafast X-ray switching. For the experiments conducted at the ESRF at an X-ray photon energy of 12 keV, this angular range extends from 14.9° to 14.75° (Fig. 3a). In order to quantitatively compare the experimental signal with theory we feed the spatio-temporal strain map calculated in a linear-chain model into a simulation of the dynamical X-ray diffraction, yielding the X-ray response of the PicoSwitch $R(t, \theta)$ (Herzog *et al.*, 2012b; Schick *et al.*, 2014). The result shows excellent agreement with the measured dynamics of the peak shift demonstrated in Fig. 3(b) and the corresponding intensity change plotted in Fig. 3(c) when keeping the angle of the PicoSwitch fixed. Fig. 3(a) shows the simulations in a broader angular range for an X-ray energy of 12 keV. The red curve represents a simulated rocking curve at a time delay of 2.25 ps after excitation. At this moment the thin SRO layer is maximally expanded. The blue curve, which is simulated for a delay of 4.74 ps, depicts the situation where the coherent compression wave has propagated into the substrate and thus terminates the coherent dynamics in the PicoSwitch.

4. Synchrotron-based pump–probe experiment

Now we apply the PicoSwitch, which was characterized in the previous section by simulations and measurements at the University of Potsdam, to a real synchrotron-based pump–probe experiment in order to study the impulsive expansion of a photo-excited metallic layer. These experiments were performed at the ID09B beamline at ESRF. The output of a Ti:sapphire laser amplifier is split into two beams in order to pump the PicoSwitch and the sample separately with delays t and τ , respectively. The pump fluence was set to 15 mJ cm^{-2} on both the PicoSwitch and the sample. A detailed schematic of the experimental set-up is shown in Figs. 4(a) and 2(b). The electronic delay t is set so that the diffraction efficiency of the

switch is turned on and off approximately when the maximum of the 100 ps X-ray pulse from the synchrotron impinges on the PicoSwitch. It is held constant during the experiment. The X-ray flux incident on the PicoSwitch was 3.4×10^{10} photons s^{-1} . The pump–probe delay τ shifts the optical pump pulse for the sample against the shortened X-ray pulse. The sample under investigation was a 70 nm metallic SRO layer grown on an STO substrate (Vrejoiu *et al.*, 2006). The dynamics in the sample can be understood in the framework of coherent phonon propagation as described before. We employ this structure as a reference to test the achievable time resolution with the gated X-ray probe pulse. The diffraction angle of the sample θ_S is set to the maximum of the SRO layer peak. After excitation of the sample with the incident optical pulse, the

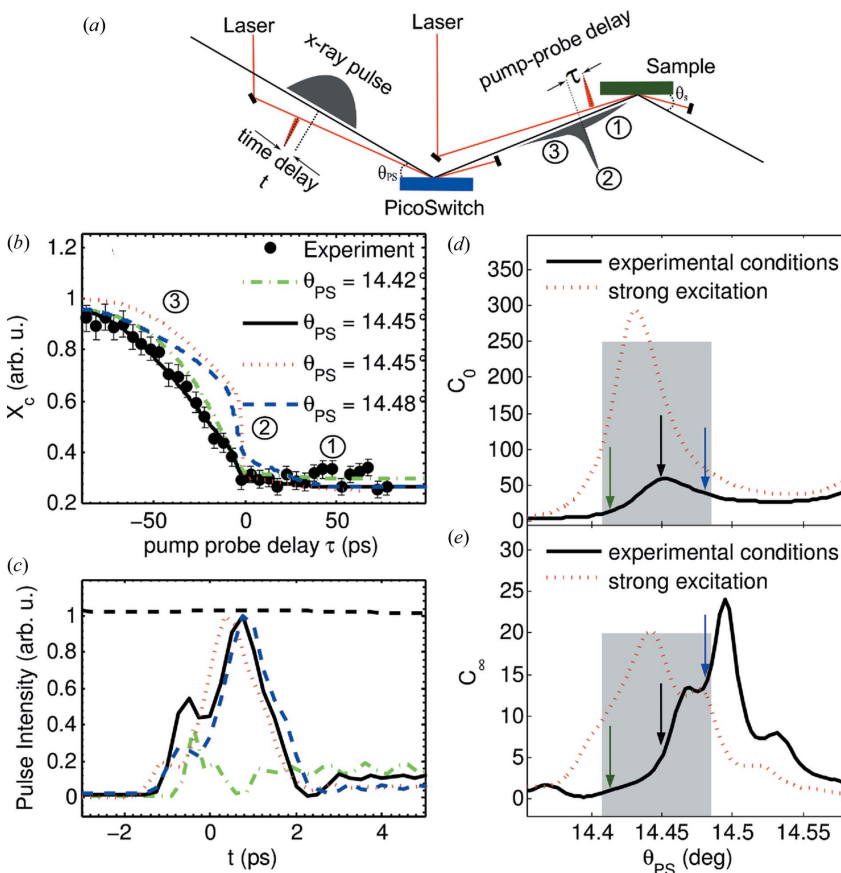


Figure 4 Synchrotron-based time-resolved experiment. (a) Sketch of the experimental set-up showing the fixed timing t of laser and X-ray pulses and the pump–probe delay τ . If the optical excitation pulse arrives earlier at the sample than the gated section of the X-ray probe pulse, the pump–probe delay τ is positive. The probe pulse is divided into three sections: leading edge (1), ultrafast gate (2) and trailing edge (3). (b) Measured (black dots) and simulated (green dash-dotted, black solid, blue dashed and red dotted lines) pump–probe correlation signal X_c . The error bars indicate a confidence interval of $\pm 32\%$. The simulations were obtained using equation (1). The angle θ_{PS} is color-coded. All simulations are for the fluence $F = 15 \text{ mJ cm}^{-2}$ used in the experiment. Only the red dotted curve is simulated for an optimized fluence of 20 mJ cm^{-2} . (c) Shortened X-ray probe pulses for different incident angles on the PicoSwitch color-coded as in (b). The black dashed line is the original X-ray probe pulse. (d) Simulated initial (C_0) and (e) final (C_∞) contrast as defined in Fig. 1 for different Bragg angles on the PicoSwitch. The black solid lines show simulations for a pump fluence of 15 mJ cm^{-2} . The red dotted lines show a contrast for stronger excitation with a fluence of 20 mJ cm^{-2} . The colored vertical arrows mark the angles where the probe pulses in (b) and (c) were calculated. The gray shaded area marks the angular resolution of the PXS measurement.

diffracted intensity decreases with a decay time of 4.5 ps, comparable with the duration of the gated X-ray pulse. Hence, the sample response is essentially a step function. Fig. 4(b) shows the measured relative change of the diffracted X-ray intensity (black bullets) as a function of the pump–probe delay τ . The green dash-dotted, black solid, red dotted and blue dashed lines represent simulations of the X-ray response assuming the simulated shortened probe pulses depicted in Fig. 4(c) with the same color code. The shape of the switched pulse is determined by the Bragg angle θ_{PS} chosen on the PicoSwitch and by the pump fluence. The simulated signals plotted as lines in Fig. 4(b) depict the normalized correlation of the sample X-ray response $R(t)$ at the fixed angle θ_S with the shortened probe pulse $P(t, \theta_{PS})$ for various diffraction angles θ_{PS} of the PicoSwitch,

$$X_c(\tau, \theta_{PS}) = \frac{\int_{-\infty}^{\infty} P(t, \theta_{PS}) R(\tau + t) dt}{\int_{-\infty}^{\infty} P(t, \theta_{PS}) R(-\infty) dt}. \quad (1)$$

5. Discussion

In the following we explain the impact of different probe pulse shapes on the measured signal. For a better understanding we divide the gated probe pulse shown in Fig. 4(a) into three sections: (1) and (3) are determined by the initial and final contrast C_0 and C_∞ , respectively, while (2) represents the ultrafast gate from the PicoSwitch. Figs. 4(b)–4(e) present the main results of the synchrotron-based optical-pump–X-ray-probe experiment with the shortened X-ray probe pulse. Experimental data are presented in Fig. 4(b) (black bullets).

Figs. 4(d) and 4(e) show the angle dependence of the initial and final contrast ratio C_0

and C_∞ , respectively. The angles θ_{PS} used in the simulations shown in Figs. 4(b) and 4(c) are marked by color-coded arrows. The black solid line is calculated for a pump fluence of 15 mJ cm^{-2} ; the red dotted line shows the contrast for a fluence of 20 mJ cm^{-2} . Note that features appearing in X_c at positive pump–probe delays stem from badly suppressed background photons in the leading edge of the probe pulse marked (1) in Fig. 4(a). Features at negative τ originate from the trailing edge of the probe pulse, which is marked (3) and is determined by the thermal relaxation of the PicoSwitch after optical pumping (Shayduk *et al.*, 2011). The sharp drop in X_c , which is observed in the red, blue and black simulation in Fig. 4(b), is caused by the short and intense section of the probe pulse and is marked (2).

Our experimental data are best reproduced by the simulation shown by the black solid line in Fig. 4(b). It shows a rather slow initial decay (3) and it is flat after the gated probe pulse (1), *i.e.* for positive τ . This indicates a large initial contrast C_0 , which is marked by the black arrow in Fig. 4(d). The sharp drop from $X_c = 0.4$ to $X_c = 0.25$ at $\tau = 0$ ps indicates the response to the ultrafast switching (2).

The simulation for larger θ_{PS} (blue dashed line) shows a lower initial and higher final contrast, leading to deviations from the observed correlation (black bullets). The dash-dotted green line shows a case where both the initial and final contrast C_0 and C_∞ are lower. The dash-dotted green probe pulse in Fig. 4(c) shows almost no ultrafast switching characteristics. Instead, the contrast ratio changes abruptly from C_0 to C_∞ . Hence, the ultrafast feature at $\tau = 0$ ps disappears and in addition there are deviations from the measured signal at negative τ . The best simulated performance could be obtained by increasing the pump fluence, as shown by the red dotted line in Figs. 4(b) and 4(c). Due to limited beam time, a corresponding measurement could not be realised. In essence, Fig. 4 shows that we have performed an ultrafast X-ray diffraction experiment with a synchrotron probe pulse which was shortened to approximately 2 ps as indicated in Fig. 4(c) by the black line.

For an optimized performance in future applications the PicoSwitch must be pumped with about 33% higher optical pump fluence. The simulation shown by the red dotted line in Figs. 4(b) and 4(c) demonstrates an increased initial and final contrast at the θ_{PS} chosen in the experiment. This parameter setting on the PicoSwitch would result in a correlation signal X_c shown by the red dotted line in Fig. 4(b). The corresponding probe pulse is shown in Fig. 4(c). The essential difference from the pulse used in the experiment is the higher contrast. The switching time is identical. For comparison, the X-ray flux of the gated pulse incident on the sample as well as the relative proportions of the sections (1)–(3) according to Fig. 4(a) are listed in Table 1.

While the PicoSwitch already allows for a significant reduction of the X-ray pulse duration, it still requires further development. In particular, the contrast ratio needs improvement in order to sufficiently suppress background photons that are reflected by the PicoSwitch in the off-state. As shown in Figs. 4(c) and 4(d), the contrast can be optimized

Table 1

X-ray flux (photons s^{-1}) and relative proportions according to Fig. 4(a) of the gated X-ray pulse for the simulations shown in Fig. 4(b).

	X-ray flux	(1)	(2)	(3)
Black solid	0.15×10^6	8%	22%	70%
Blue dashed	0.18×10^6	22%	38%	40%
Red dotted	2.8×10^6	7%	48%	45%

through the diffraction angle on the PicoSwitch and through the excitation fluence on the device. The main impediment to increasing the contrast is the lattice expansion due to laser heating of the device. Hence, the final contrast C_∞ is the limiting parameter. The contrast can be improved by changing the PicoSwitch structure from a thin film to a heterostructured multilayer. In such a structure one layer could be employed for the generation of a coherent expansion and compression wave that would propagate into neighboring layers. There, the central angle of the Bragg reflection would be shifted according to the modification of the lattice spacing, allowing for the same type of switching as was demonstrated in our experiment. Since the propagation of the strain wave occurs significantly faster than thermal diffusion, the switching would be almost free of thermal background distortion.

However, our experiment shows that the PicoSwitch is suitable for generating probe pulses that are capable of resolving ultrafast dynamics on a few-picosecond timescale. We would like to point out that the PicoSwitch can sustain even higher fluences up to 40 mJ cm^{-2} without degradation. The generated X-ray pulses are limited in duration to a few picoseconds and are therefore longer than the pulses obtained through slicing of the electron bunch. The achievable photon flux is comparable. However, the PicoSwitch experiment is significantly easier to implement. The temporal stability and angular resolution of the gated X-rays are determined by the synchrotron source. This is a significant advantage compared with laser plasma sources, such as the PXS at the University of Potsdam. We think that the PicoSwitch could be employed to improve the performance of synchrotron sources for time-resolved experiments in the future.

6. Conclusion

In conclusion, we have characterized and applied an ultrafast X-ray switch for gating synchrotron X-ray pulses on picosecond timescales. The shape of the shortened pulse can be adjusted by selecting the Bragg angle on the switch and by tuning the pump fluence. The switching relies on coherent phonon dynamics which modulate the diffraction efficiency. The rise and fall times t_r and t_f are determined by the layer thickness and the speed of sound in the material. We demonstrated a high switching contrast with a maximum diffraction efficiency of $\eta_{\text{max}} \simeq 10^{-3}$. The structure allows for repetitive switching and no long-term degradation effects have yet been observed. Hence, the device is suited for permanent installation in time-resolved beamline set-ups. The applicability of the PicoSwitch was demonstrated in a synchrotron-

based pump–probe experiment where we measured coherent lattice dynamics in a nanostructured sample with picosecond resolution.

We thank the BMBF for funding the project *via* 05K10IP1.

References

- Abo-Bakr, M., Feikes, J., Holldack, K., Wüstefeld, G. & Hübers, H. W. (2002). *Phys. Rev. Lett.* **88**, 254801.
- Allam, D. (1970). *J. Phys. E*, **3**, 1022.
- Als-Nielsen, J. (2011). *Elements of Modern X-ray Physics*, 2nd ed. New York: John Wiley and Sons.
- Bargheer, M., Zhavoronkov, N., Woerner, M. & Elsaesser, T. (2006). *ChemPhysChem*, **7**, 783–792.
- Beaud, P., Johnson, S. L., Streun, A., Abela, R., Abramsohn, D., Grolimund, D., Krasniqi, F., Schmidt, T., Schlott, V. & Ingold, G. (2007). *Phys. Rev. Lett.* **99**, 174801.
- Bucksbaum, P. H. & Merlin, R. (1999). *Solid State Commun.* **111**, 535–539.
- Cammarata, M., Eybert, L., Ewald, F., Reichenbach, W., Wulff, M., Anfinrud, P., Schotte, F., Plech, A., Kong, Q., Lorenc, M., Lindenau, B., Rübiger, J. & Polachowski, S. (2009). *Rev. Sci. Instrum.* **80**, 015101.
- Chang, Z., Rundquist, A., Zhou, J., Murnane, M. M., Kapteyn, H. C., Liu, X., Shan, B., Liu, J., Niu, L., Gong, M. & Zhang, X. (1996). *Appl. Phys. Lett.* **69**, 133–135.
- Emma, P. *et al.* (2010). *Nat. Photon.* **4**, 641–647.
- Enquist, H., Navirian, H., Nüske, R., von Korff Schmising, C., Jurgilaitis, A., Herzog, M., Bargheer, M., Sondhauss, P. & Larsson, J. (2010). *Opt. Lett.* **35**, 3219–3221.
- Geloni, G., Saldin, E., Samoylova, L., Schneidmiller, E., Sinn, H., Tschentscher, T. & Yurkov, M. (2010). *New J. Phys.* **12**, 035021.
- Grigoriev, A., Do, D.-H., Kim, D. M., Eom, C.-B., Evans, P. G., Adams, B. & Dufresne, E. M. (2006). *Appl. Phys. Lett.* **89**, 021109.
- Herzog, M., Bojahr, A., Goldshteyn, J., Leitenberger, W., Vrejoiu, I., Khakhulin, D., Wulff, M., Shayduk, R., Gaal, P. & Bargheer, M. (2012a). *Appl. Phys. Lett.* **100**, 094101.
- Herzog, M., Leitenberger, W., Shayduk, R., van der Veen, R., Milne, C. J., Johnson, S. L., Vrejoiu, I., Alexe, M., Hesse, D. & Bargheer, M. (2010). *Appl. Phys. Lett.* **96**, 161906.
- Herzog, M., Schick, D., Gaal, P., Shayduk, R., von Korff Schmising, C. & Bargheer, M. (2012b). *Appl. Phys. A*, **106**, 489–499.
- Navirian, H. A., Herzog, M., Goldshteyn, J., Leitenberger, W., Vrejoiu, I., Khakhulin, D., Wulff, M., Shayduk, R., Gaal, P. & Bargheer, M. (2011). *J. Appl. Phys.* **109**, 126104.
- Pile, D. (2011). *Nat. Photon.* **5**, 456–457.
- Rousse, A., Rischel, C. & Gauthier, J.-C. (2001). *Rev. Mod. Phys.* **73**, 17–31.
- Schick, D., Bojahr, A., Herzog, M., von Korff Schmising, C., Shayduk, R. & Bargheer, M. (2014). *Comput. Phys. Commun.* **185**, 651–660.
- Schick, D., Bojahr, A., Herzog, M., von Korff Schmising, C., Shayduk, R., Leitenberger, W., Gaal, P. & Bargheer, M. (2012). *Rev. Sci. Instrum.* **83**, 025104.
- Schick, D., Shayduk, R., Bojahr, A., Herzog, M., von Korff Schmising, C., Gaal, P. & Bargheer, M. (2013). *J. Appl. Cryst.* **46**, 1372–1377.
- Schoenlein, R. W., Chattopadhyay, S., Chong, H. H., Glover, T. E., Heimann, P. A., Shank, C. V., Zholents, A. A. & Zolotorev, M. S. (2000). *Science*, **287**, 2237–2240.
- Shayduk, R., Navirian, H. A., Leitenberger, W., Goldshteyn, J., Vrejoiu, I., Weinelt, M., Gaal, P., Herzog, M., von Korff Schmising, C. & Bargheer, M. (2011). *New J. Phys.* **13**, 093032.
- Sheppard, J. M. H., Sondhauss, P., Merlin, R., Bucksbaum, P. H., Lee, R. W. & Wark, J. S. (2005). *Solid State Commun.* **136**, 181–185.
- Sokolowski-Tinten, K., Horn von Hoegen, M., von der Linde, D., Cavalleri, A., Siders, C. W., Brown, F. L. H., Leitner, D. M., Toth, C., Squier, J. A., Barty, C. P. J., R., Wilson, K. R. & Kammler, M. (2001). *J. Phys. IV*, **11**, Pr2-473–Pr2-477.
- Vrejoiu, I., Le Rhun, G., Pintilie, L., Hesse, D., Alexe, M. & Gösele, U. (2006). *Adv. Mater.* **18**, 1657–1661.
- Wark, J. S., Whitlock, R. R., Hauer, A. A., Swain, J. E. & Solone, P. J. (1989). *Phys. Rev. B*, **40**, 5705–5714.
- Zamponi, F., Ansari, Z., von Korff Schmising, C., Rothhardt, P., Zhavoronkov, N., Woerner, M., Elsaesser, T., Bargheer, M., Trobitzsch-Ryll, T. & Haschke, M. (2009). *Appl. Phys. A*, **96**, 51–58.
- Zholents, A., Heimann, P., Zolotorev, M. & Byrd, J. (1999). *Nucl. Instrum. Methods Phys. Res. A*, **425**, 385–389.
- Zolotoyabko, E. & Quintana, J. P. (2004). *Rev. Sci. Instrum.* **75**, 699–708.